—資　料—

Effect of Different Lung Material in One-Design Cardiac Phantom on Myocardial SPECT Images

Kotatsu Tsuboi[1)], Masahisa Onoguchi[2)], Takayuki Shibutani[2)], Akio Nagaki[3)] and Kei Tsukamoto[1)]

1) Department of Radiological Technology, Hamamatsu Red Cross Hospital
2) Department of Quantum Medical Technology, Institute of Medical, Pharmaceutical and Health Sciences, Kanazawa University
3) Department of Radiological Technology, Kurashiki Central Hospital

(article received : Jan 7, 2022)

Key words: Individual difference, Cardiac phantom, Lung material, SPECT, RH-2

1. Introduction

Myocardial perfusion single-photon emission computed tomography (MPS) images depend on acquisition methods, such as collimator, acquisition time, orbit type, pixel size, and matrix size[1~4)], and image reconstruction methods[5)]. Moreover, different acquisition and image reconstruction methods are established by each institution[6)]. Therefore, previous phantom studies have investigated the differences in myocardial defect size and quantitative indices of left ventricular (LV) function on different gamma camera systems[7~12)]. The effects of cardiac phantom differences must be clarified to perform a high-accuracy phantom study.

In Japan, a commercial cardiac phantom owned by a radiopharmaceutical manufacturer is commonly used while performing a study using a phantom. The RH-2 model cardiac phantom uses the following two types of materials in the lungs: sponge and wood powder. These materials have been widely used in most commercial cardiac phantoms in Japan[13~15)] and other countries[16~18)]. The materials of the lung field cannot be selected by the experimenter unless the materials of the lung field of the phantom provided by the pharmaceutical manufacturer are selected by the experimenter. The differences in the lung materials of the phantom may affect MPS image quality due to different photon attenuation. Some guidelines recommended performing computed tomography (CT)-based attenuation correction (CTAC) with the ordered subset expectation maximization method[19,20)]. However, MPS examination in Japan performed CTAC in only 43.4% of the institutions using ^{99m}Tc solution[21)]. Therefore, the influence of attenuation for two different lung materials in phantoms is greatly important for understanding the image quality, and quantitative indices in the phantom study, including single-photon emission CT (SPECT) scanner, cannot perform the CTAC.

This study aimed to validate the effect of different lung materials in one-design cardiac phantom on myocardial SPECT images.

2. Materials and Methods

2-1. Cardiac phantom

Seventeen cardiac phantoms (Model RH-2; Kyoto Kagaku, Kyoto, Japan) were used. The acrylic thickness of the outer container and myocardial thickness according to information from Kyoto Kagaku are 10 mm. The phantoms were composed of the normal myocardium, spine, and lungs. The material of the lung field was sponge type in nine phantoms and wood powder type in eight phantoms, and the lung was not filled with water. The myocardium was filled with 90.0 kBq/mL of ^{99m}Tc solution. The mediastinum, left chamber cavity, and right ventricle were filled with nonradioactive water.

2-2. Acquisition and image processing

2-2-1. CT

The phantoms were acquired on a 64-detector CT scanner (LightSpeed VCT; GE Healthcare, Waukesha, WI, USA). The scanning parameter were as follows: tube voltage, 120 kVp; tube current, 3D mA modulation; detector collimation, 64 × 0.625 mm; helical pitch, 1.375; gantry rotation time, 0.5 s; acquisition of 1.25 mm images reconstructed at 1.25 mm intervals; scan field of view, 50.0 cm; display field of view, 36.0 cm; matrix, 512 × 512; and standard reconstruction kernel. The outer container size, acrylic thickness of the outer container and myocardium, CT number of the lung, and LV volume were measured using Synapse Vincent (version 5.5; Fujifilm Corp., Tokyo, Japan).

2-2-2. SPECT

SPECT acquisition was performed using a dual-detector gamma camera (E.CAM signature; Canon, Tokyo, Japan). The SPECT images were acquired using low-energy high-resolution collimator with an energy window of 140 keV ± 7.5%, opposite each detector configuration, 64 × 64 matrix, 1.45 zooming, with 60 projections, circular orbit of 360°, and pixel size of 6.59 mm. The projection data were acquired for 30 s per projection.

The SPECT images were reconstructed with the filtered back projection method using a ramp filter as reconstruction filter and Butterworth filter as prefilter with cut-off frequency of 0.42 cycles/cm and order of 8. Neither scatter nor attenuation correction was performed. We used the Heart Risk View-Score version 8.0 (Nihon Medi-Physics, Tokyo, Japan) to create a polar map[22,23]. The LV volume was calculated automatically using quantitative perfusion SPECT (QPS) version 4.0 (Cedars-Sinai Medical Center, CA, USA)[24].

2-3. Image evaluation

We measured the major axis, minor axis, and height dimensions of the outer container and acrylic thickness of the outer container using CT images at five points (top, right, bottom, oblique, and left) (**Fig. 1**). From the short axis of the CT images, the slice of the apical, mid, and base was determined so that the long axis of the LV was divided into four parts. The myocardial thickness of the anterior, septal, inferior, and lateral regions was measured in each slice. The myocardial thickness of the apex was also measured from the LV long axis image (**Fig. 2**). A 500 mm^2 rectangular region of interest was placed in both the lung fields of the CT image; following this, the CT number was calculated from the average of five slices centered on the heart.

The polar map was normalized to 100% peak activity, and the relative ratio (%) of gamma ray count uptake (%uptake) was assessed for each segment. The %uptake was compared with those of segments 17, 13-16, 7-12, and 1-6 of the 17-segmment model polar map as apex, apical, mid, and base, respectively[25]. Moreover, %uptake was calculated from the five-segment model polar map as anterior, septal, inferior, lateral, and apex regions; %uptake of each segment was compared. The LV volume was calculated by extracting the LV cavity from the CT image and from the short axis of the SPECT image.

2-4. Statistical analysis

All statistical analyses were performed using EZR version 1.40 (Saitama Medical Center, Jichi Medical University, Saitama, Japan), which is a graphical user interface for R (The R Foundation for Statistical Computing, Vienna, Austria). More precisely, EZR is a modified version of the R commander, designed to add statistical functions that are frequently used in biostatistics[26].

We used Student's t-test to examine the effect of different components in the lungs on the size and acrylic thickness of the outer container, myocardial thickness, CT number, LV volume, and %uptake. However, Welch test was used only for the anterior region of the five-segment model polar map because the F-test did not show equal variance between the two groups. Kruskal-Wallis test was used to compare

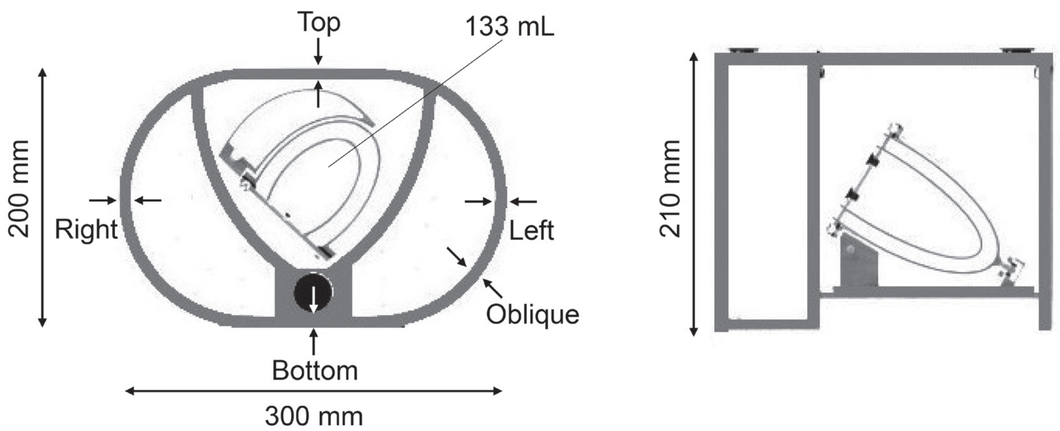

Fig. 1 Diagrams of RH-2 type phantom. The left and right images are the superior and oblique views. Major axis, minor axis, height, and left ventricular volume are nominal values.

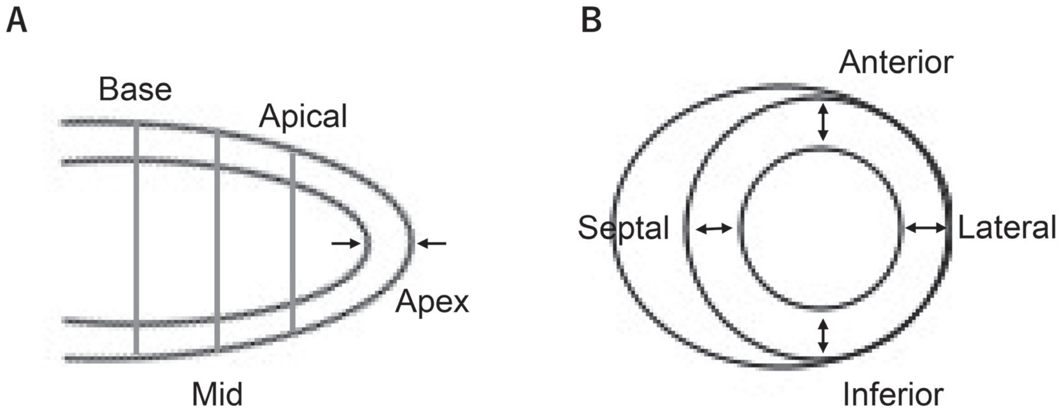

Fig. 2 Measurement points using computed tomography images of the apex (arrowhead), and slice positions of the apical, mid, and base (A). Measurement points of the anterior, septal inferior, and lateral regions (B).

myocardial thickness and %uptake in the apex, apical, mid, and base, followed by Bonferroni correction for two-by-two comparisons.

In all analyses, a P-value of <0.05 indicated statistical significance.

3. Results

The dimensions and acrylic thickness of the outer container showed no difference in all measurement points between sponge and wood powder types (**Table 1** and **2**). The myocardial thickness also showed no difference in all measurement points between sponge and wood powder types (**Table 3**). The apex was thicker than the other regions in both sponge and wood powder types (**Fig. 3**).

The CT numbers of the lung were -927.2 ± 12.4 HU in the sponge type and -679.4 ± 14.1 HU in the wood powder type ($P<0.001$). The CT number of the wood powder type was higher than that of the sponge type.

The %uptake of the 17-segment model polar map was significantly higher in the apical, mid, and base in the sponge type than in the wood powder type (**Table 4**). The %uptake of the apex was higher than that of other positions in both sponge and wood powder types (**Fig. 4**). The sponge type had a higher %uptake of the inferior region than the wood powder type ($72.1 \pm 4.9\%$ versus $67.0 \pm 2.5\%$; $P<0.05$). (**Table 5**, **Fig 5**).

The LV volumes calculated from CT data for

Table 1 Comparison of dimensions of outer container using computed tomography images

	Sponge type (mm)	Wood powder type (mm)	*P* value
Major axis	299.5 ± 0.5	299.4 ± 0.6	*NS* (0.79)
Minor axis	199.5 ± 0.6	199.1 ± 0.7	*NS* (0.25)
Height	209.0 ± 0.5	208.9 ± 0.9	*NS* (0.36)

NS : not significant

Table 2 Comparison of acrylic thickness of outer container using computed tomography images

	Sponge type (mm)	Wood powder type (mm)	*P* value
Top	8.7 ± 0.3	8.8 ± 0.2	*NS* (0.36)
Right	8.3 ± 0.2	8.3 ± 0.2	*NS* (0.58)
Bottom	8.3 ± 0.1	8.4 ± 0.2	*NS* (0.29)
Left	8.5 ± 0.2	8.4 ± 0.1	*NS* (0.36)
Oblique	8.6 ± 0.1	8.7 ± 0.3	*NS* (0.56)

NS : not significant

Table 3 Comparison of thickness of the myocardial region using computed tomography images

	Sponge type (mm)	Wood powder type (mm)	*P* value
Apex	10.5 ± 0.9	11.0 ± 0.6	*NS* (0.20)
Apical	9.3 ± 0.7	9.4 ± 0.6	*NS* (0.39)
Mid	9.7 ± 0.5	9.8 ± 0.5	*NS* (0.39)
Base	9.7 ± 0.5	9.8 ± 0.5	*NS* (0.42)
Anterior	9.5 ± 0.6	9.6 ± 0.5	*NS* (0.45)
Septal	9.7 ± 0.5	9.7 ± 0.5	*NS* (0.97)
Inferior	9.3 ± 0.6	9.5 ± 0.5	*NS* (0.43)
Lateral	9.8 ± 0.6	10.0 ± 0.6	*NS* (0.24)

NS : not significant

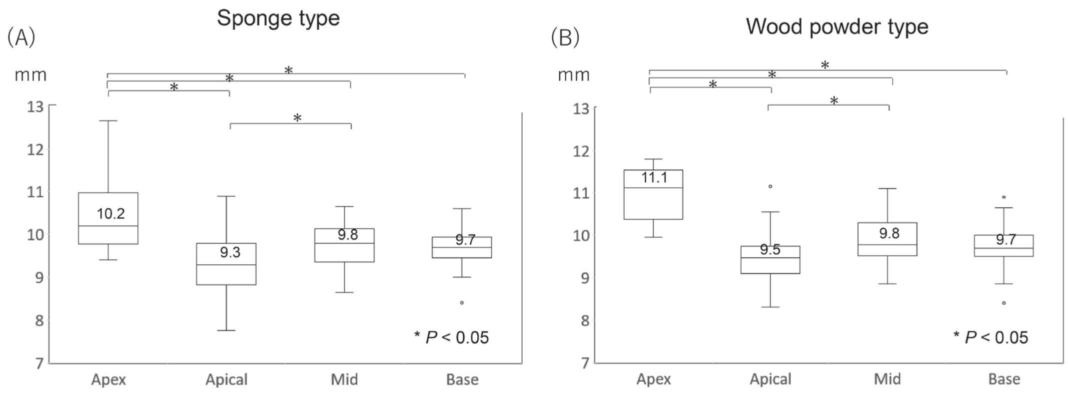

Fig. 3 Myocardial thickness using computed tomography images for sponge type (A) and wood powder type (B)

Table 4　Comparison of %uptake of 17-segment model polar map between sponge type and wood powder type

	Sponge type (mm)	Wood powder type (mm)	*P* value
Apex (seg. 17)	83.7±2.7	83.1±1.7	*NS* (0.614)
Apical (seg. 13–16)	75.1±5.7	72.4±3.9	0.026*
Mid (seg. 7–12)	73.2±4.8	70.4±3.2	<0.001**
Base (seg. 1–6)	71.5±4.8	67.8±2.6	<0.001**

NS : not significant
* : $P<0.05$
** : $P<0.001$

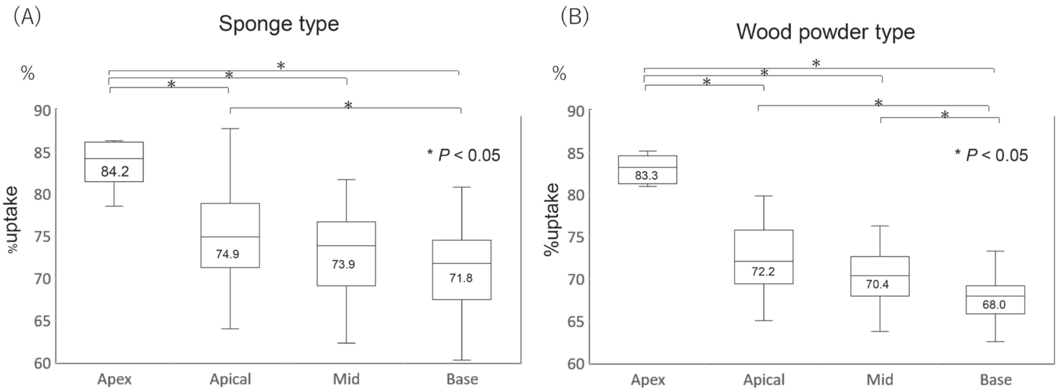

Fig. 4　Comparison of %uptake calculated from 17-segment model polar map for sponge type (A) and wood powder type (B)

Table 5　Comparison of %uptake of 5-segment model polar map between sponge type and wood powder type

	Sponge type (mm)	Wood powder type (mm)	*P* value
Anterior	73.1±4.8	71.0±2.1	*NS* (0.27)
Septal	74.2±4.7	71.0±2.1	*NS* (0.12)
Inferior	72.1±4.9	67.0±2.5	<0.05*
Lateral	73.0±3.7	70.6±2.8	*NS* (0.16)

NS : not significant
* : $P<0.05$

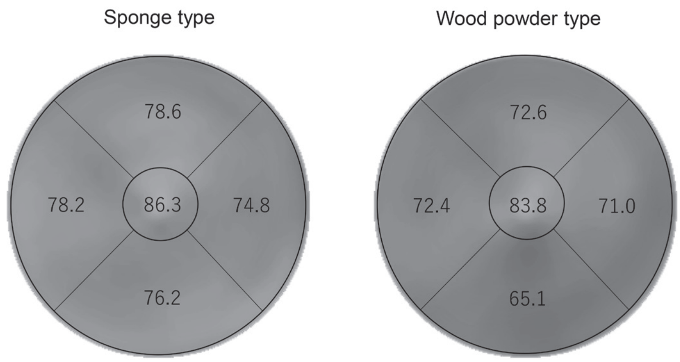

Fig. 5　Example of five-segment model polar map. Visually, the inferior region of wood powder type is lower than that in the sponge type. Values for %uptake are overlaid on polar maps.

sponge and wood powder types were 130.2 ± 10.4 mL and 133.9 ± 3.6 mL, respectively (P = 0.065). The LV volumes calculated from SPECT data for sponge and powder types were 159.6 ± 3.7 mL and 156.9 ± 2.4 mL, respectively (P = 0.105). The LV volume between sponge and wood powder types was not significantly different in both CT and SPECT images.

4. Discussion

Even with one-design cardiac phantoms, the %uptake of the inferior wall depends on individual differences among phantoms due to different attenuations of the lung material.

The individual differences of one-design phantom may affect MPS images. Nevertheless, few studies have attempted to clarify the effect of the individual differences for one-design phantom on MPS images. RH-2 model cardiac phantom with two types of different materials in the lungs is widely used in Japan[13~15]. We need to confirm that phantoms with lung fields of different materials can be used to perform correct evaluations. The acrylic thickness and myocardial thickness showed no difference between the sponge and wood powder types. The lung materials are commonly constructed using polystyrene beads and interstitial radioactive water, and their lung density is typically −640 HU[27]. The absence of water or radioactive water in the lung fields might cause lower lung density of both sponge and wood powder types. The difference in the attenuation coefficient calculated from CT value for the sponge and wood powder types in the lung is 0.037 cm^{-1} [28]. We hypothesized that the difference in the attenuation coefficient caused a greater difference in photon attenuation than a statistical error. The heart region of the phantom used in this study is surrounded by the lungs. Consequently, the basal inferior myocardial wall is more affected by the attenuation of the lung field due to its location in the deep torso[29]. Conversely, the apex is closer to the detector and is less susceptible to attenuation by the lung field[30]. The phantom material and difference in the photon attenuation between the sponge and wood powder in the lung field were responsible for the lower %uptake in the apical, mid, and base in the 17-segment model polar map and inferior region in the five-segment model polar map. All myocardial thicknesses designed by the manufacturer's information were constant at 10 mm. However, we demonstrated that the myocardial thickness of the apex was thicker than that of the other regions. The %uptake of the apex between the sponge and wood powder showed no difference because the myocardial wall thickness at the apex was similar. However, the apex showed relatively high %uptake because the wall thickness of the apex is thicker than that of other myocardial walls, which resulted in a relatively low value for the other myocardial walls. The relatively high uptake in the apex may have clarified the difference in photon attenuation by lung field materials. Therefore, the %uptake at the inferior wall between the sponge and wood powder showed a significant difference.

Attenuation correction with CTAC for myocardial SPECT is not commonly performed in Japan[21]. If several phantoms of the same design are used, choosing the same lung material is critical for accurate image quality evaluation. Furthermore, the LV volume calculated by QPS was not affected by attenuation due to differences in lung field material. Thus, the LV volume can be evaluated using several phantoms with different lung fields.

This study has several limitations. We validated individual differences in one-design cardiac phantoms using only one gamma camera at one facility. However, myocardial SPECT used different acquisition and image reconstruction methods in each gamma camera in a phantom study. The differences of a collimator and acquisition orbit and the use of spatial resolution correction affect the myocardial perfusion distribution[1,3,9]. In many phantom studies, the lung fields simulate air[1,2,6~8]. Moreover, the uptake in the lung fields is much lower than in the myocardium, liver, and other organs. Therefore, we did not use the phantom with nonradioactive water in the lung field. However, the nonradioactive water in the lung field may affect the distribution of myocardium due to attenuation and scattering effects. Further studies are needed to address these issues.

5. Conclusion

The individual differences among the one-design cardiac phantoms affect the myocardial perfusion distribution due to the different attenuations between sponge and wood powder types. The one-design cardiac phantom should use the same lung material for assessing MPS images in a series of phantom studies.

Disclosure

No potential conflict of interest relevant to this article was reported.

Acknowledgment

We thank Hidetoyo Nishida and Hideki Nishiyama of Nihon Medi-Physics Co., Ltd. for providing RH-2 model cardiac phantom.

References

1) Armstrong IS, Saint KJ, Tonge CM, et al. Evaluation of general-purpose collimators against high-resolution collimators with resolution recovery with a view to reducing radiation dose in myocardial perfusion SPECT: A preliminary phantom study. J Nucl Cradiol 2017; **24**(2): 596–604
2) Ramos SM, Glavam AP, Kubo TT, et al. Optimization of a protocol for myocardial perfusion scintigraphy by using an anthropomorphic phantom. Radiol Bras 2014; **47**(4): 217–222
3) Liu YH, Lam PT, Sinusas AJ, et al. Differential effect of 180 degrees and 360 degrees acquisition orbits on the accuracy of SPECT imaging: quantitative evaluation in phantoms. J Nucl Med 2002; **43**(8): 1115–24
4) Nakajima K, Taki J, Higuchi T, et al. Gated SPET quantification of small hearts: mathematical simulation and clinical application. Eur J Nucl Med 2000; **27**(9): 1372–9
5) Bruyant PP. Analytic and iterative reconstruction algorithms in SPECT. J Nucl Med 2002; **43**(10): 1343–1358
6) Heikkinen J, Ahonen A, Kuikka JT, et al. Quality of myocardial perfusion single-photon emission tomography imaging: multicentre evaluation with a cardiac phantom. Eur J Nucl Med 1999; **26**(10): 1289–97
7) O'Connor MK, Gibbons RJ, Juni JE, et al. Quantitative myocardial SPECT for infarct sizing: feasibility of a multicenter trial evaluated using a cardiac phantom. J Nucl Med 1995; **36**(6): 1130–6
8) O'Connor MK, Leong LK, Gibbons RJ. Assessment of infarct size and severity by quantitative myocardial SPECT: results from a multicenter study using a cardiac phantom. J Nucl Med 2000; **41**(8): 1383–10
9) Zoccarato O, Scabbio C, De Ponti E, et al. Comparative analysis of iterative reconstruction algorithms with resolution recovery for cardiac SPECT studies. A multi-center phantom study. J Nucl Cardiol 2014; **21**(1): 135–48
10) Ronkainen AP, Eneh CTM, Linder PH, et al. Assessment of ejection fraction and heart perfusion using myocardial perfusion single-photon emission computed tomography in Finland and Estonia: a multicenter phantom study. Nucl Med Commun 2020; **41**(9): 888–895
11) O'connor MK, Kemp B, Anstett F, et al. A multicenter evaluation of commercial attenuation compensation techniques in cardiac SPECT using phantom models. J Nucl Cardiol 2002; **9**(4): 361–76
12) Vebene HJ, Schneider PD, Spijkerboer A, et al. Multicenter intercomparison assessment of consistency of left ventricular function from a gated cardiac SPECT phantom. J Nucl Cardiol 2006; **13**(6): 801–10
13) Funahashi M, Shimonagata T, Mihara K, et al. Application of pixel truncation to reduce intensity artifacts in myocardial SPECT imaging with Tc-99m tetrofosmin. J Nucl Cardiol 2002; **9**(6): 622–31
14) Tanaka R, Yoshioka K, Seino K, et al. New software for raw data mask processing increases diagnostic ability of myocardial SPECT imaging. Ann Nucl Med 2011; **25**(4): 231–9
15) Onishi H, Matsutomo N, Kangai Y, Saho T, Amijima H. Differential impact of multi-focus fan beam collimation with L-mode and conventional systems on the accuracy of myocardial perfusion imaging: Quantitative evaluation using phantoms. Asia Ocean J Nucl Med Biol 2013; **1**(2): 28–34
16) Gibbons RJ, Verani MS, Behrenbeck T, et al. Feasibility of tomographic ^{99m}Tc-hexakis-2-methoxy-2-methylpropyl-isonitrile imaging for the assessment of myocardial area at risk and the effect of treatment in acute myocardial infarction. Circulation 1989;

80(5):1277–86
17) Knesaurek K. A new dual-isotope convolution cross-talk correction method: a Tl-201/Tc-99m SPECT cardiac phantom study. Med Phys 1994;**21**(10): 1577–83
18) Knešaurek K, Machac J. Comparison of ^{18}F SPECT with PET in myocardial imaging: a realistic thorax-cardiac phantom study. BMC Nucl Med 2006; **31**(6), https://doi.org/10.1186/1471-2385-6-5
19) Dorbala S, Ananthasubramaniam K, Armstrong IS, et al. Single Photon Emission Computed Tomography (SPECT) Myocardial Perfusion Imaging Guidelines: Instrumentation, Acquisition, Processing, and Interpretation. J Nucl Cardiol 2018; **25**(5): 1784–1846
20) Verberne HJ, Acampa W, Anagnostopoulos C, et al. EANM procedural guidelines for radionuclide myocardial perfusion imaging with SPECT and SPECT/CT: 2015 revision. Eur J Nucl Med Mol Imaging 2015; **42**(12): 1929–40
21) Shibutani T, Okuda K, Ichikawa H, et al. Imaging technology for myocardial perfusion single-photon emission computed tomography 2018 in Japan. Jpn J Radiol 2020; **38**(3): 274–282
22) Iwasaki T, Kurisu S, Abe N, et al. Validation of automated quantification of myocardial perfusion single-photon emission computed tomography using Heart Score View in patients with known or suspected coronary artery disease. Int Heart J 2014; **55**(4): 350–6
23) Nakata T, Hashimoto A, Matsuki T, et al. Prognostic value of automated SPECT scoring system for coronary artery disease in stress myocardial perfusion and fatty acid metabolism imaging. Int J Cardiovasc Imaging 2013; **29**(1): 253–62
24) Germano G, Kavanagh PB, Waechter P, et al. A new algorithm for the quantitation of myocardial perfusion SPECT. I: technical principles and reproducibility. J Nucl Med 2000; **41**(4): 712–9
25) Cerqueira MD, Weissman NJ, Dilsizian V, et al. Standardized myocardial segmentation and nomenclature for tomographic imaging of the heart. A statement for healthcare professionals from the Cardiac Imaging Committee of the Council on Clinical Cardiology of the American Heart Association. Int J Cardiovasc Imaging, J Nucl Cardio 2002; **9**(2): 240–5
26) Kanda Y. Investigation of the freely available easy-to-use software 'EZR' for medical statistics. Bone Marrow Transplant 2013; **48**(3): 452–8
27) Lehnert AL, Hunter WC, McDougald WA, et al. Development and testing of SPECT/CT lung phantoms made from expanding polyurethane foam. Med Phys 2019; **46**(12): 5593–5601
28) Patton JA, Turkington TG. SPECT/CT physical principles and attenuation correction. J Nucl Med Technol 2008; **36**(1): 1–10
29) Tonge CM, Manoharan M, Lawson RS, et al. Attenuation correction of myocardial SPECT studies using low resolution computed tomography images. Nucl Med Commun 2005; **26**(3): 231–7
30) Burrell S, MacDonald A. Artifacts and pitfalls in myocardial perfusion imaging. J Nucl Med Technol 2006; **34**(4): 193–211